Current Applied Physics 13 (2013) 1899–1905

Contents lists available at ScienceDirect

Current Applied Physics

journal homepage: www.elsevier.com/locate/cap

Compensation of stray capacitance of the quartz tuning fork for a quantitative force spectroscopy

Sangmin An, Kunyoung Lee, Bongsu Kim, Jongwoo Kim, Soyoung Kwon, Qhwan Kim, Manhee Lee [1], Wonho Jhe*

Center for Nano-Liquid, Department of Physics and Astronomy, Seoul National University, Seoul 151-747, Republic of Korea

ARTICLE INFO

Article history:
Received 22 March 2013
Received in revised form
27 July 2013
Accepted 30 July 2013
Available online 9 August 2013

Keywords:
Quartz tuning fork (QTF) sensor
TP-QTF
Stray capacitance compensation (SCC)
Confined nano-water

ABSTRACT

We have introduced a simple but robust approach to realize stray-capacitance compensation of a quartz tuning fork force gradient sensor by using a tied-prong of the same tuning fork instead of using a variable precision capacitor. The results of quantitative force measurements with the proposed device show excellent agreement with the numerical method of cancellation via the theoretical compensation method with the resonance response curves. Futhermore, the mechanical properties of the condensed nano-water bridges are investigated with the proposed compensator, which provides the potential promise of the intrinsic quartz tuning fork for a quantitative precision force spectroscopy.

1. Introduction

Quartz tuning forks (QTF) have been used as a highly sensitive tip in atomic force microscopes (AFM) due to several advantages they possess, such as their small size, high quality factor (*Q*-factor) in ambient conditions and non-optical (electrical) detection of the signal [1–6], after Karrai et al. first reported them in 1995 [7]. Moreover, several kinds of atomic images (Si-111, mica, and so on) were successfully obtained with the QTF adopted AFM system in various environments (vacuum, liquid, ambient conditions) [8–13]. However, there is a limitation to their direct adoption in a quantitative force measurement system for use in interpreting the interaction force as a simple harmonic oscillator, due to non-harmonic behavior by the stray capacitance from the two electrodes conducted on the quartz crystal. There have been several efforts to overcome this limitation, for example using a theoretical compensation method [14], the usage of single prong of QTF (tying the other prong onto the rigid body), namely a qPlus sensor [15], or a stray capacitance compensation (SCC) circuit with a variable capacitor [16]. In this paper, we introduced the SCC with a tied-prong (TP) of the QTF which gives another solution of SCC and high performance quantitative measurement alternative as a force gradient sensor to a variable capacitor. Additionally, a study of confined nano-water was performed with a proposed SCC system with TP-QTF for sensing a small force interaction [17] instead of the q-plus sensor, whose *Q*-factor is insufficient to detect small perturbations in ambient conditions. With this simple technique, one can easily apply the model of a simple harmonic oscillator in the interpretation of interactions with high *Q*-factors (~10,000).

2. Methods

2.1. SCC system with TP-QTF

A tied-prong of the QTF is proposed as the critical component for overcoming the non-harmonic behavior arising from the stray capacitance of the QTF. Fig. 1(a) shows a circuit diagram for SCC of the QTF with TP-QTF. The driving signal of a continuous wave from the function generator (Agilent, 33120A) branches to the QTF sensor and TP-QTF after inverting the phase. The circuit model of the QTF sensor consists of a harmonic oscillator (Part 1, phase of 90°) represented by the model of LRC series and stray capacitance (Part 2, phase of 0°). Thus, the current signal from stray capacitance (Part 2) and TP-QTF whose value of stray capacitance is nearly same and of opposite phase of 180° compared to that of Part 2 cancel each other out. And only the current signal of harmonic oscillating

* Corresponding author.
E-mail address: whjhe@snu.ac.kr (W. Jhe).
URL: http://cnl.snu.ac.kr
[1] Present address: S. LSI, Giheung-Campus, Samsung Electronics, Republic of Korea.

1567-1739/$ – see front matter © 2013 Elsevier B.V. All rights reserved.
http://dx.doi.org/10.1016/j.cap.2013.07.024

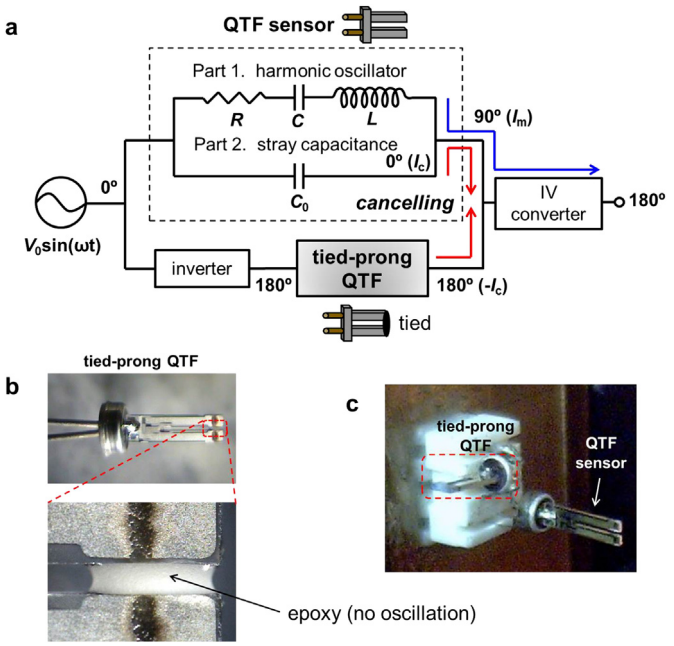

Fig. 1. SCC with TP-QTF. The current from stray capacitance (Part 2) and TP-QTF whose value of stray capacitance is nearly same and of opposite phase compared to that of Part 2 cancel each other out. (a) Circuit diagram for SCC of the QTF with TP-QTF. (b) Image of TP-QTF. The legs are fixed by gluing with epoxy for no oscillation. (c) Image of proposed device in practical experiment.

motion is left and converted to voltage by *IV*-converter with the phase of 90°. Note that the stray capacitances of the randomly selected QTFs from the product lot have slightly different values, even the fabrication process is same. In this experiment, we choose 50 EA sample of TP-QTF which has a standard deviation value of ~1.25 ± 0.2 pF in same lot with random selection. For perfect compensation of stray capacitance, one has to find the exact same value of stray capacitance of QTF, which is difficult to realize in practice. However, with the standard deviation value, we can derive and regulate the interaction force of elasticity and viscosity which mentions in the nano-water experiment within error bound.

Based on the electrical circuit model which is based on the theoretical SCC 14 with suppression of the stray capacitance term (I_c), $C_0 \sim 0$, the output electrical current is described by the mechanical amplitude (A_m) and phase (θ_m) of the QTF sensor, which values are nearly same ($I_c = I_{qc} - I_{tpqc} \sim 0$) with the variation of the electrical amplitude (A_e) and phase (θ_e) with the cancellation of the stray capacitance effect as follows:

$$I_m = A_m \sin(\omega t + \theta_m) = I_e - I_c = I_e - \underline{(I_{qc} - I_{tpqc})} \sim A_e \sin(\omega t + \theta_e), \tag{1}$$

$$A_m (\sim A_e) \sim \frac{I_0 \omega}{Q \omega_0} \sqrt{\frac{1}{\left(1 - \omega^2/\omega_0^2\right)^2 - \left(\omega/(\omega_0 Q)\right)^2}}, \tag{2}$$

$$\theta_m (\sim \theta_e) \sim \arg\left[\frac{\omega}{\omega_0 Q} + i\left(1 - \frac{\omega^2}{\omega_0^2}\right)\right], \tag{3}$$

where I_m, I_e, I_c are each output signal of mechanical, electrical current, and total stray capacitance of QTF which is compensated by mixing the stray capacitance of target QTF sensor (I_{qc}) and TP-QTF (I_{tpqc}). $\omega_0 (=1/LC)$ and ω are the resonance and driving frequencies, $I_0 = V_0/R$, and $Q = (\omega_0 L/R)$ is the Q-factor. Fig. 1(b) shows the captured image of TP-QTF. The edges of each prong were glued by epoxy for the purpose of inhibiting oscillatory motion and contribution of stray capacitance. Fig. 1(c) shows the image of the proposed device in a practical experiment. The AFM sharp tip is attached to the edge of one prong of the QTF sensor, and approaches the sample varying the distance by the piezoelectric transducer (PZT). Additionally, the TP-QTF is placed near the QTF sensor for SCC under the same experimental conditions.

Fig. 2 shows the frequency, time domain amplitude (current) and phase signal of the QTF sensor in order to understand the non-harmonic motion of intrinsic QTF. The frequency domains of each point (①–⑦) of part 1, part 2, and QTF sensor are placed with the time domains on the right side of the figure. The current of part 1 is

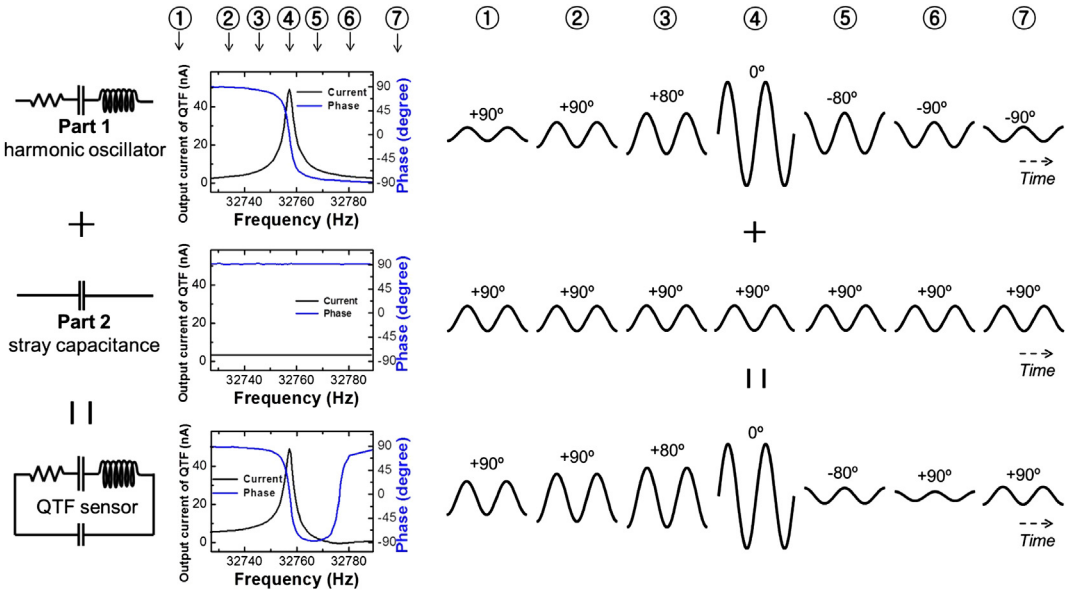

Fig. 2. Frequency and time domain amplitude and phase signal of the QTF sensor. The electrical current of the QTF sensor shows constructive interference with a similar phase in the downward region before the resonance frequency (④), while destructive interference with a different phase exerted in the upward region after the resonance frequency.

gradually changed until point ③; however, the signal is drastically changed to the opposite phase toward −90° experience near resonance frequency at point ④, while that of part 2 is fixed in the phase of 90°. Thus, the output current of the QTF sensor shows constructive interference with the similar phase in the downward region (①–③) before the resonance frequency at the spot of ④, while that destructive interference with a different phase is exerted in the upward region (⑤–⑦) after the resonance frequency. As the component of part 2 is removed, the interaction force on the QTF sensor can be interpreted by a model of a simple harmonic oscillator for a quantitative force measurement sensor.

2.2. Performance of the proposed SCC system

Fig. 3 shows the performances of the proposed SCC system with TP-QTF along with a comparison of an intrinsic QTF and theoretical SCC. Fig. 3(a) and (b) shows the validation of inhibiting oscillatory motion of TP-QTF to figure out the minimum vibration amplitude. Fig. 3(a) shows the resonance curves (log plot) of intrinsic QTF ($I_m + I_c$) and the same QTF of SCC with TP-QTF ($I_c \sim 0$) after the fabrication process with epoxy is done (frequency sweeping range; 10 kHz ($f_0 \pm 5$ kHz)). Inset shows magnified graph near the resonance frequency ($f_0 \pm 50$ Hz), which indicates the inhibiting oscillatory motion of TP-QTF. In addition, it is difficult to find the evidence of the TP-QTF's resonance peak is occurred, even the driving amplitude increases from 100 mV to 400 mV using a function generator in Fig. 3(b). Thus, the SCC of QTF sensor can be realized with combining with the inverting current signal of TP-QTF at least in condition of confined nano-water experiment which range of driving amplitude is typically 100–400 mV. Fig. 3(c) and (d) shows the resonance curves of the QTF in three cases (intrinsic QTF, SCC theory and TP-QTF), which are plotted by measurement of a lock-in amplifier (EG&G, 7265) with respect to the frequency sweeping ranges of 100 Hz ($f_0 \pm 50$ Hz) and 10 kHz ($f_0 \pm 5$ kHz, for wide range validation) using a function generator (Agilent, 33120A). Each linear plot shows Lorentzian line shape resonance curve of SCC using theory and TP-QTF, while the intrinsic QTF shows inharmonic behavior. We could clearly observe the differences with each inset log scale graphs which indicate that the simple harmonic oscillator can be used in the experiment with the matched results between theoretical SCC and SCC with TP-QTF. The measured Q-factor is about 10,000. The Q-factor is important to

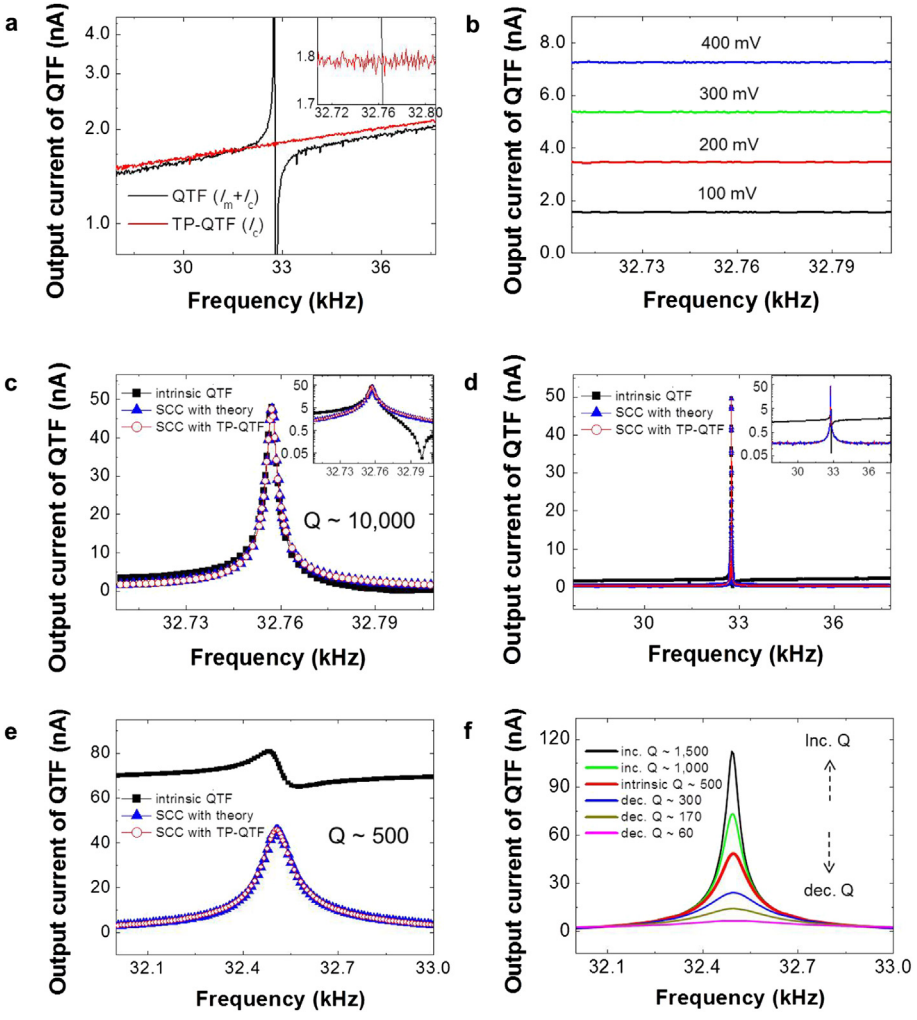

Fig. 3. Performances of the proposed SCC system with TP-QTF. (a) Resonance curves of intrinsic QTF ($I_m + I_c$) and the same QTF of SCC with TP-QTF ($I_c \sim 0$) (sweeping range; f_0 ±5 kHz), which indicates the inhibiting oscillatory motion of TP-QTF. (b) Resonance curves by increment of driving amplitude of resonance peak (sweeping range; f_0 ±50 Hz). (c)–(d) The resonance curves of the QTF in three cases are plotted by measurement of a lock-in amplifier (EG&G, 7265) with respect to the frequency sweeping ranges of 100 Hz (f_0 ±50 Hz) and 10 kHz (f_0 ±5 kHz, for wide range validation) using a function generator (Agilent, 33120A) in the case of Q-factor ~10,000. (e) Comparison with resonance curves between the intrinsic QTF and SCC system with TP-QTF in the case of Q-factor 500. The stray capacitance of intrinsic QTF contributes to suppression of the control of the Q-factor. (f) Increment and decrement of the Q-factor by the active-Q controller in the case of SCC with TP-QTF.

detect the sensitive interactions of small perturbations in various environments of the practical experiment. However, in the case of low *Q*-factor of the intrinsic QTF in Fig. 3(e) (< ~500), control of the *Q*-factor by the active-*Q* controller is not available, because the stray capacitance, which is in the opposite phase, also receives electrical gain by the loop of the controller, enough to influence the output current of the QTF sensor. Thus, the mechanical current signal cannot obtain enough gain to increase or decrease the *Q*-factor. Conversely, in the case of SCC with TP-QTF of which only the harmonic signal survives, the gain loop of the active-*Q* controller can completely control the *Q*-factor. Fig. 3(f) shows the increment and decrement of the *Q*-factor in the case of SCC with TP-QTF, which is easily controlled by the variable resistor of the active-*Q* controller from ~10 to ~30,000 in ambient conditions, which circuit is demonstrated by Jahng et al. in the case high *Q*-factor of QTF [18,19].

3. Results and discussions

3.1. Study of confined nano-water using SCC system with TP-QTF

Confined nano-water plays an important role in biological processes [20–22], and thus its mechanical properties need to be investigated. Fig. 4 shows the setup of the confined nano-water experiment with a shear-mode QTF–AFM system. The nano-water meniscus, which forms naturally between the AFM tip and the mica substrate by capillary condensation [17], was studied and shown in Fig. 4(a). The shape of the water meniscus is well-established without a jump-to-contact instability due to the high stiffness of the QTF, which commonly occurs in conventional cantilever-based AFM. The prong of the QTF oscillates laterally at the surface (shear-mode) for the sole purpose of detecting the interactions of the water meniscus, without sensing the perpendicularly interacting forces, such as van der Waals and electrostatic forces. The AFM tip, which is fabricated by a commercial puller (P-2000, Sutter Instrument Co.) with a diameter of ~500 nm was attached to the end of the QTF's prong by epoxy. The approach speed was about 0.1 nm/s, and the oscillation amplitude of the tip apex was about 0.5 nm, which value is obtained by measurement of current amplitude with respect to the captured real images of QTF sensor's oscillating amplitude using a stroboscope-combined optical microscope [23] in Fig. 4(b). The

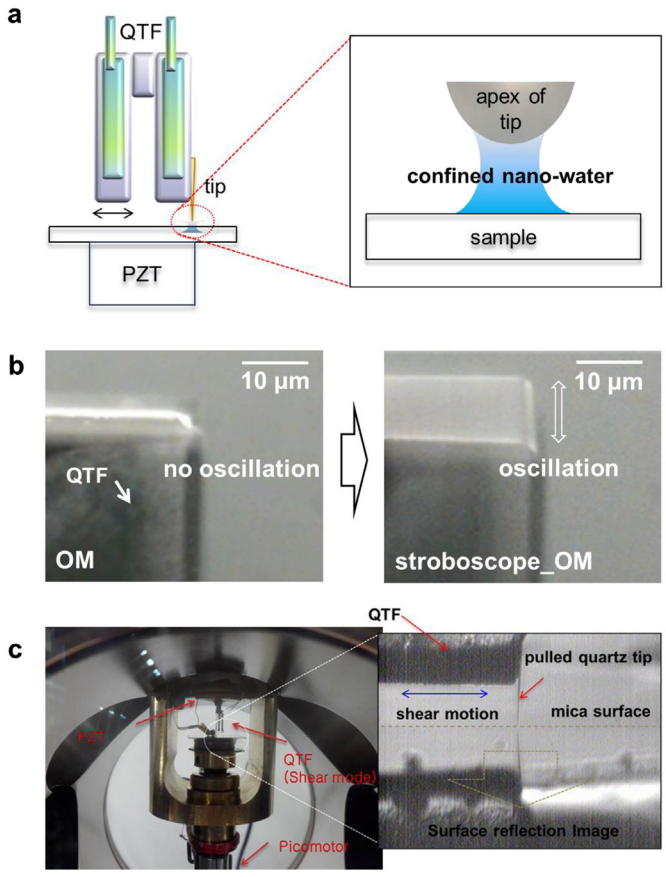

Fig. 4. Apparatus for study of the confined nano-water using the shear-mode QTF-AFM system. (a) Schematic of the setup. The nano-water meniscus is formed between the AFM tip and the mica substrate by capillary condensation. (b) Stroboscope-combined OM images for definition of real value of QTF's oscillating amplitude. (c) Picture of the setup. The tip can be easily approach the surface closely by monitoring the surface reflection image (rough) and the amplitude signal of QTF (fine). The metal chamber is facilitated to sustain the relative humidity and temperature.

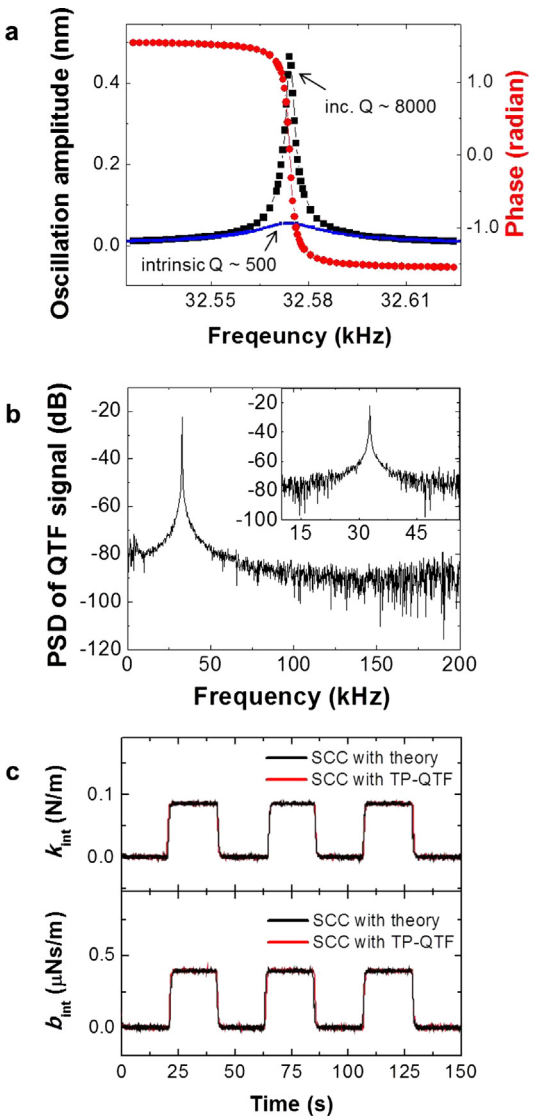

Fig. 5. Definition of the QTF-AFM probe system. (a) Harmonic motion of the prong of the QTF sensor using SCC system with TP-QTF. The *Q*-factor is increased up to 8000 from 500. (b) Power spectral density (noise floor) of the AFM tip attached TP-QTF. (c) Modulated effective elasticity and damping by an artificially perturbed interaction force using theoretical SCC and SCC system with TP-QTF.

current value derived by the captured image of oscillation amplitude gives the information of real amplitude of the QTF. The mica substrate was chemically cleansed after *in situ* cleavage. Fig. 4(c) shows the picture of the experimental setup. The AFM tip easily approaches the surface within 10 nm distance from the surface by a PZT with a high vertical resolution (0.1 nm). The tip can easily approach the surface closely by monitoring the surface reflection image (rough) and the amplitude signal of QTF (fine). Moreover, the metal chamber facilitates sustaining the relative humidity (46.1 ± 0.3%) and temperature (23.2 ± 0.1 °C) which are critical factors in this experiment. The measured thermal drift was about 0.53 pm/s.

3.2. Interpretation of the nano-water's mechanical properties using the proposed system

The mechanical properties of the confined nano-water can be interpreted with a model of a simple harmonic oscillator using SCC system with TP-QTF based on the amplitude [24,25] and frequency [26] detection method in the case of a small oscillation. In this experiment, the amplitude modulation (AM) mode QTF-AFM was used, including a calculation of the elasticity and viscosity of the nano-water. Fig. 5(a) represents a harmonic motion of the prong of the QTF sensor using SCC system with TP-QTF. The *Q*-factor of the intrinsic QTF sensor with a value of ~500 was increased to ~8000

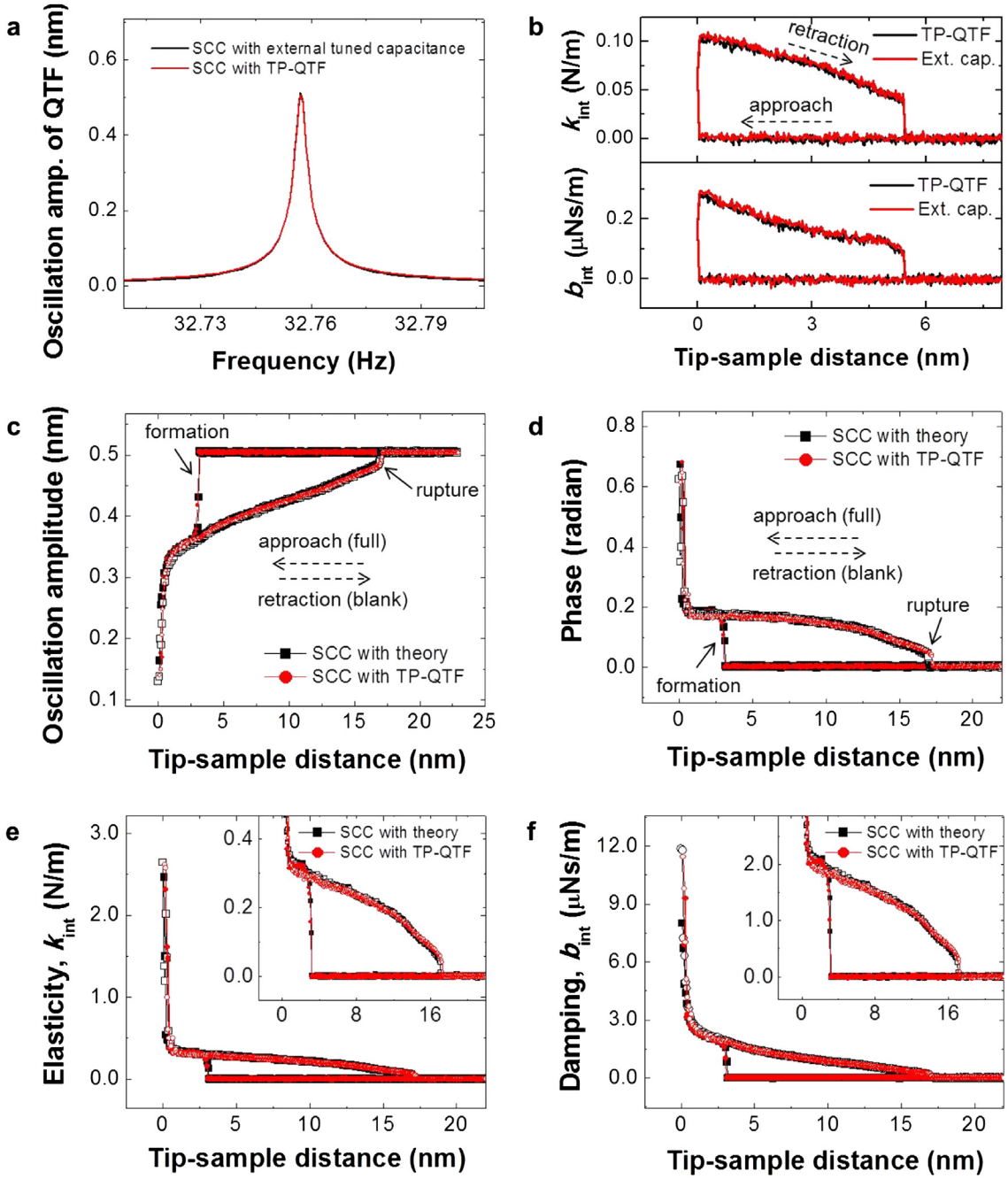

Fig. 6. Viscoelasticity of confined nano-water using SCC system with TP-QTF. (a)–(b) Comparative measurements with external tuned capacitance. (c)–(d) Approach/retraction curves of amplitude and phase of QTF sensor. Each curve between the theoretical SCC and SCC with TP-QTF are well matched. (e)–(f) Calculated effective elasticity and damping curves.

by the active-*Q* controller for the purpose of sensitive detection of small interaction forces. The variations of amplitude and phase express the damping by interactions and the changed effective stiffness of the target materials, respectively. In addition, the power spectral density (noise floor) of the AFM tip attached TP-QTF was checked with several times using the dynamic signal analyzer (Agilent, 35670A) in Fig. 5(b) (inset graph is the magnified plot for short range of the frequency). The measured signal-to-noise ratio of the system is about 58 dB. The active version of *IV*-converter noise was superimposed onto the overall electrical output signal of the AFM probe system with current background noise of $\sim$0.13 pA Hz$^{-1/2}$. The effective elasticity (k_{int}) and damping (b_{int}) related to viscosity are modulated by changing the artificially interacted elastic and viscous forces, as shown in Fig. 5(c). The artificially applied interactions of k_{int} and b_{int} are induced from the frequency and amplitude variations of the function generator, respectively, for the purpose of pre-assumption of interaction force's mechanical properties. The variation of k_{int} is dealt with the change of frequency shift of the QTF sensor by the interaction force, while the b_{int} is varied by the interacted damping force with the variation of QTF sensor's amplitude. The calculated values of elasticity and damping using the theoretical SCC and SCC with TP-QTF are well matched with each other. The viscoelasticity of the confined nano-water can be derived from the model of a damped harmonic oscillator as follows: $k_{\mathrm{int}} = F/A \sin\theta + m\omega^2 - k$, $b_{\mathrm{int}} = F/(A\omega)\cos\theta - b$, where A and θ are the measured amplitude and phase of the QTF sensor, m is an effective mass, k (=27439.2 N/m) is a spring constant of the QTF sensor, b ($=k/(Q\omega_0)$) is a damping coefficient, F ($=kA_0/Q$) is the amplitude of driving force, and A_0 is a free oscillation amplitude.

3.3. Viscoelasticity of the confined nano-water

Now we focus on the confined nano-water experiment with this well-defined apparatus. Two kinds of experiment (SCC with TP-QTF vs. external tuned capacitance and theoretical SCC) are performed. Fig. 6(a) and (b) shows results of comparative measurements with external tuned capacitance. Both resonance curves (Fig. 6(a)) and effective elasticity/damping of SCC with external tuned capacitance and TP-QTF are good fit with each other. When the tip approaches the surface within a few nanometer, the amplitude (damping) and phase (effective elasticity) signals of QTF sensor suddenly changes by formation of the capillary-condensed nano-water meniscus. And then the tip retracts immediately and ruptured. The resonance frequency of QTF sensor is about $\sim$32757.2 Hz. These similar results indicate the validation of SCC with TP-QTF. Current device has a weakness of when the electrode lead becomes long (>10 cm), the current is drastically attenuated. In this case of TP-QTF can be facilitated close to the QTF sensor, thus, the SCC of QTF sensor can be clearly performed without degradation of current signal of TP-QTF. Moreover, the TP-QTF facilitates on the system, there is no need to tuning the capacitance for preparation of experiment every time. Fig. 6(c) and (d) shows the approach/retraction curves which are typically used to define the mechanical properties of the target materials. When the AFM tip approaches the surface, the amplitude and phase of the QTF sensor are suddenly changed at $\sim$3 nm away from the surface due to the formation of a nano-water bridge, and approaches further to define the absolute distance ($\sim$0 nm) from the surface until the signal is drastically changed by contact. Then the tip is immediately retracted in the opposite direction of the surface, finally the water meniscus is ruptured at $\sim$14 nm away from the spot of formation, which distance is used to calculate the volume of the water meniscus ($\sim$1544.2 nm^3) [27]. Each data point was drawn with reproducibly obtained average values over 30 repetitions. Fig. 6(e) and (f) shows the plotted effective elasticity and damping values of each point given by calculation of the amplitude and phase of the QTF sensor based on the developed theory of the confined nano-water's viscoelasticity [28]. Each value between the theoretical SCC and SCC with TP-QTF are well matched. The measured effective elasticity and damping of the confined nano-water are $\sim$0.28 N/m and $\sim$1.8 μNs/m at the spot of formation, respectively (inset). And the effective elasticity and damping suddenly increase near the surface, which may be caused by a phase transition of the confined nano-water (under preparation for publication). Note that the values of elasticity and viscosity gradually decrease until a rupture in the process of retraction, due to the distance-dependent variation of the contact line (tip–water–air) and contact area (tip–water) under the conditions of a fixed volume of the water meniscus (inset). The calculated damping of small oscillations was about 15 times greater than the hydrodynamic damping of bulk water [29]. This may be attributed to the enhanced value of the water viscosity within the confined geometry of a nano-gap.

4. Conclusion

We have shown that the SCC system with TP-QTF can be used as a force gradient sensor, removing non-harmonic effects for the study of confined nano-water, allowing sensitive and quantitative dynamic force spectroscopy in ambient conditions. Nevertheless, defining the exact same stray capacitance of TP-QTF & QTF sensor is still unsolved problem, this well-established simple method may contribute to improve several electric-field induced mechanical systems (sensors, actuators, or resonator) by removing the unwilling non-linear effect of stray capacitance. Moreover, one may be further extended to the quantitative mechanical study of nano-biological materials, such as cells, DNA, and proteins in various environments.

Acknowledgments

This work was supported by a National Research Foundation of Korea (NRF) grant funded by the Korea government (MEST) (2012-047677) and the Brain Korea 21.

References

[1] F.J. Giessibl, Rev. Mod. Phys. 75 (2003) 949–983.
[2] J.A. Hedberg, A. Lal, Y. Miyahara, P. Grütter, G. Gervais, M. Hilke, L. Pfeiffer, K.W. West, Appl. Phys. Lett. 97 (2010) 143107.
[3] L. González, J. Otero, G. Cabezas, M. Puig-Vidal, Sens. Actuators A 184 (2012) 112–118.
[4] J. Polesel-Maris, C. Lubin, F. Thoyer, J. Cousty, J. Appl. Phys. 109 (2011) 074320.
[5] J. Welker, F. de Faria Elsner, F.J. Giessibl, Appl. Phys. Lett. 99 (2011) 084102.
[6] A. Castellanos-Gomez, N. Agraït, G. Rubio-Bollinger, Ultramicroscopy 111 (2011) 186–190.
[7] K. Karrai, R.D. Grober, Appl. Phys. Lett. 66 (1995) 1842.
[8] Y. Seo, H. Choe, W. Jhe, Appl. Phys. Lett. 83 (2003) 1860–1862.
[9] F.J. Giessibl, Science 267 (1995) 68–71.
[10] L.P. Van, V. Kyrylyuk, F. Thoyer, J. Cousty, J. Appl. Phys. 104 (2008) 074303.
[11] Y. Liu, R. DiFoggio, K. Sanderlin, L. Perez, J. Zhao, Sens. Actuators A 167 (2011) 347–353.
[12] E. Wutscher, F.J. Giessibl, Rev. Sci. Instrum. 82 (2011) 093703.
[13] J. Otero, L. Gonzalez, M. Puig-Vidal, Sensors 12 (2012) 4803–4819.
[14] M. Lee, J. Jahng, K. Kim, W. Jhe, Appl. Phys. Lett. 91 (2007) 023117.
[15] F.J. Giessibl, Appl. Phys. Lett. 73 (1998) 3956–3958.
[16] Y. Qin, R. Reifenberger, Rev. Sci. Instrum. 78 (2007) 063704.
[17] H. Choe, M.-H. Hong, Y. Seo, K. Lee, G. Kim, Y. Cho, J. Ihm, W. Jhe, Phys. Rev. Lett. 95 (2005) 187801.
[18] J. Jahng, M. Lee, H. Noh, Y. Seo, W. Jhe, Appl. Phys. Lett. 91 (2007) 023103.
[19] J. Jahng, M. Lee, C. Stambaugh, W. Bak, W. Jhe, Phys. Rev. A 84 (2011) 022318.
[20] M.S. Cheung, A.E. García, J.N. Onuchic, Proc. Natl. Acad. Sci. 99 (2002) 685–690.
[21] Y. Levy, J.N. Onuchic, Proc. Natl. Acad. Sci. 101 (2004) 3325–3326.
[22] Y.J. Jeon, H. Kim, S. Jon, N. Selvapalam, D.H. Oh, I. Seo, C.-S. Park, S.R. Jung, D.-S. Koh, K. Kim, J. Am. Chem. Soc. 126 (2004) 15944–15945.
[23] A. Castellanos-Gomez, N. Agraït, G. Rubio-Bollinger, Nanotechnology 20 (2009) 215502.

[24] M. Lee, W. Jhe, Phys. Rev. Lett. 97 (2006) 036104.
[25] Y. Seo, W. Jhe, Rep. Prog. Phys. 71 (2008) 016101.
[26] S. An, J. Kim, K. Lee, B. Kim, M. Lee, W. Jhe, Appl. Phys. Lett. 101 (2012) 053114.
[27] C.D. Willett, M.J. Adams, S.A. Johnson, J.P.K. Seville, Langmuir 16 (2000) 9396–9405.
[28] M. Lee, B. Sung, N. Hashemi, W. Jhe, Faraday Discuss. 141 (2009) 415–421.
[29] O.I. Vinogradova, Langmuir 11 (1995) 2213–2220.